Supplemental Information

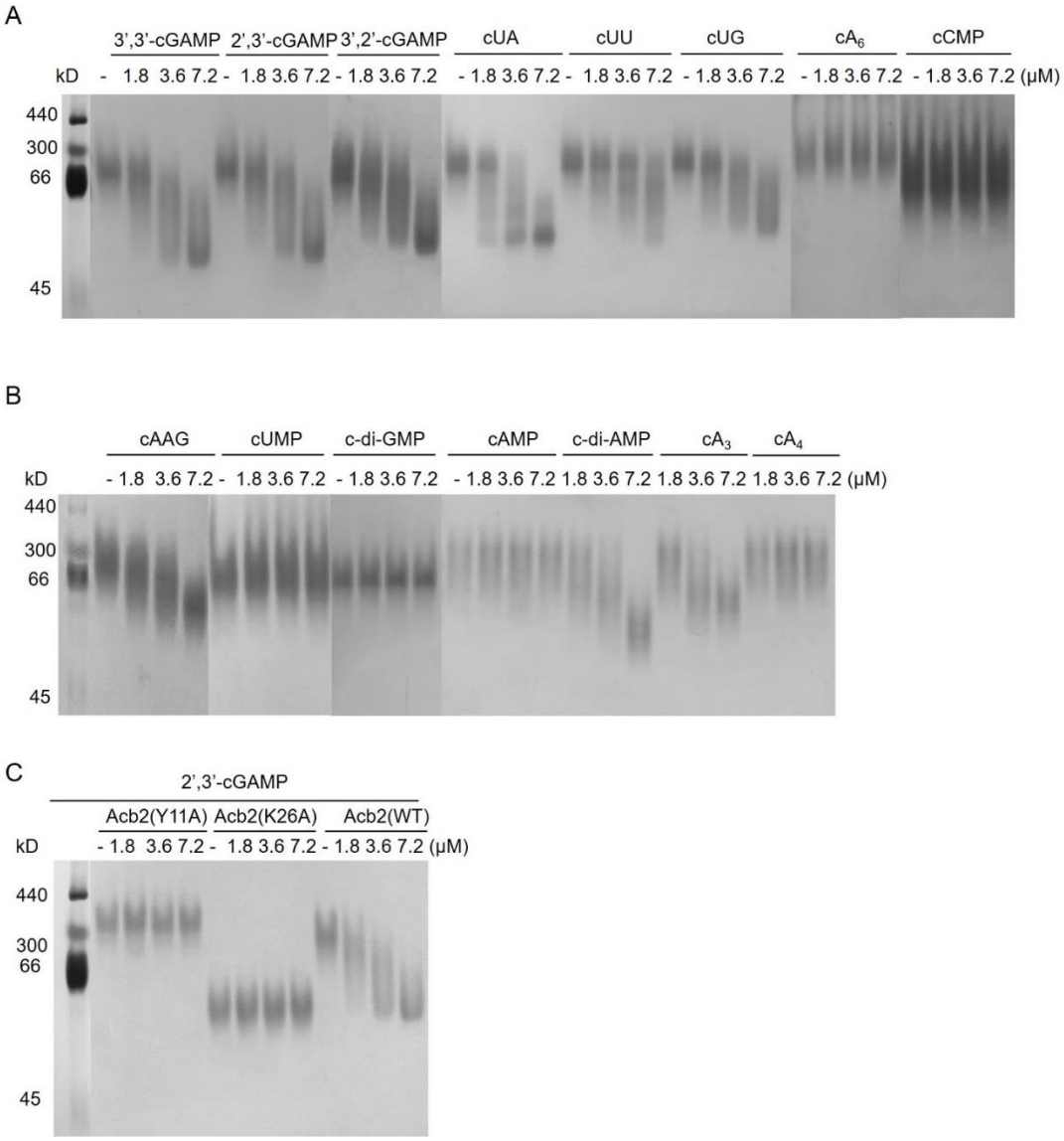

Figure S1. The cyclic nucleotide binding spectrum of PaMx33-Acb2, related to Figures 1 and 2

(A-C) Native PAGE assay showed the binding of PaMx33-Acb2 and its mutants to cyclic nucleotides.

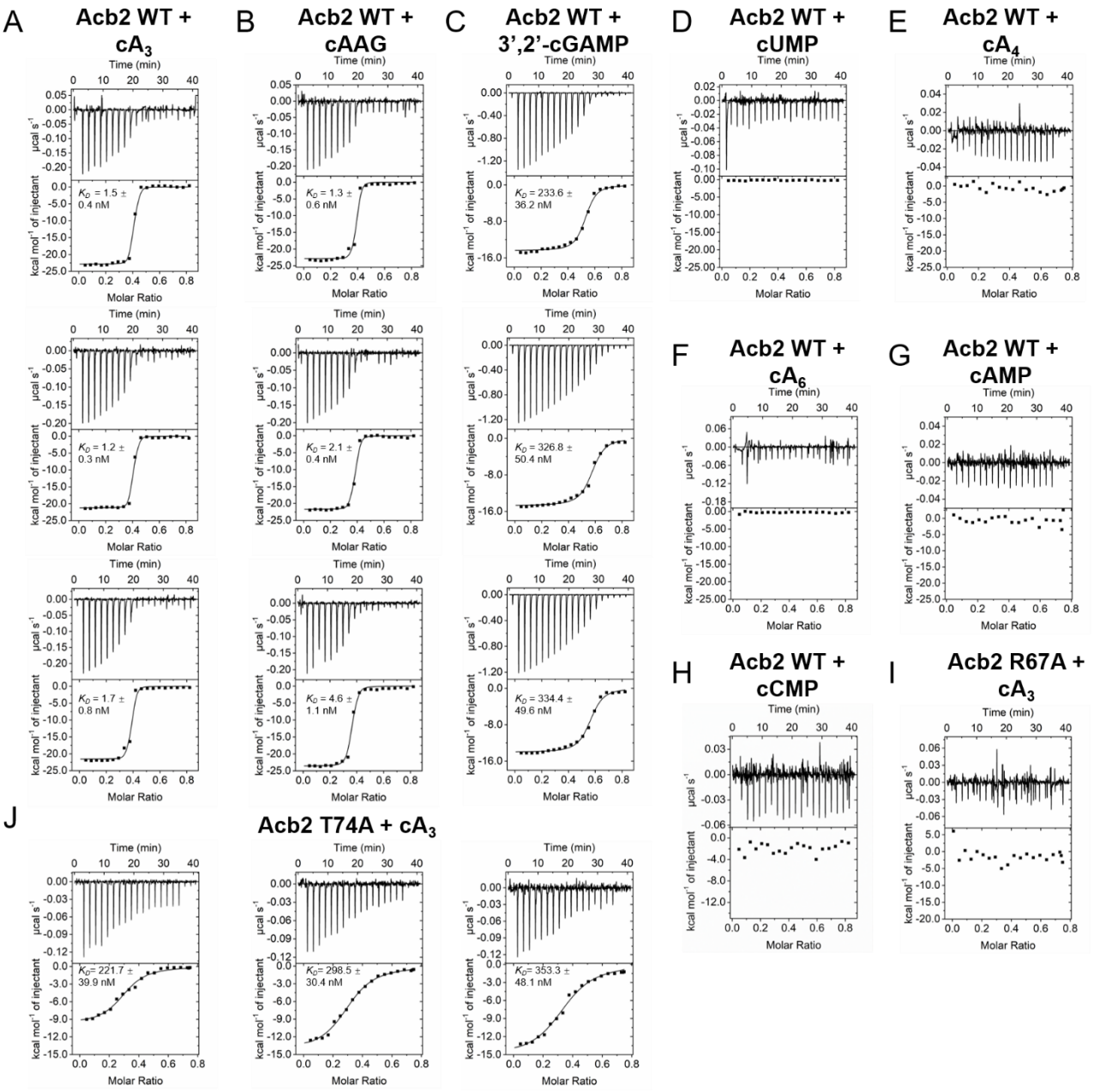

Figure S2. The binding spectrum of PaMx33-Acb2 studied by ITC assays, related to Figures 1 and 2

(A-H) ITC assays to test binding of PaMx33-Acb2 to cyclic nucleotides.

(I-J) ITC assays to test binding of cA_3 to PaMx33-Acb2 T74A and PaMx33-Acb2 R67A.

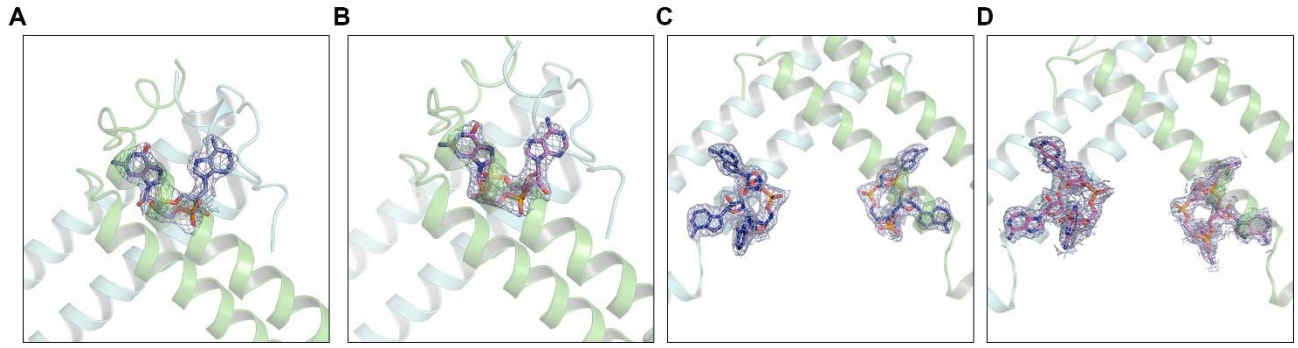

Figure S3. Density map of bound nucleotides in the structures of this study, related to Figures 1 and 2

2Fo-Fc electron density of 3',2'-cGAMP, 2',3'-cGAMP, cA_3 and cAAG within the structures of Acb2-3',2'-cGAMP, Acb2-2',3'-cGAMP, Acb2-cA3 and Acb2-cAAG contoured at 1 σ, respectively.

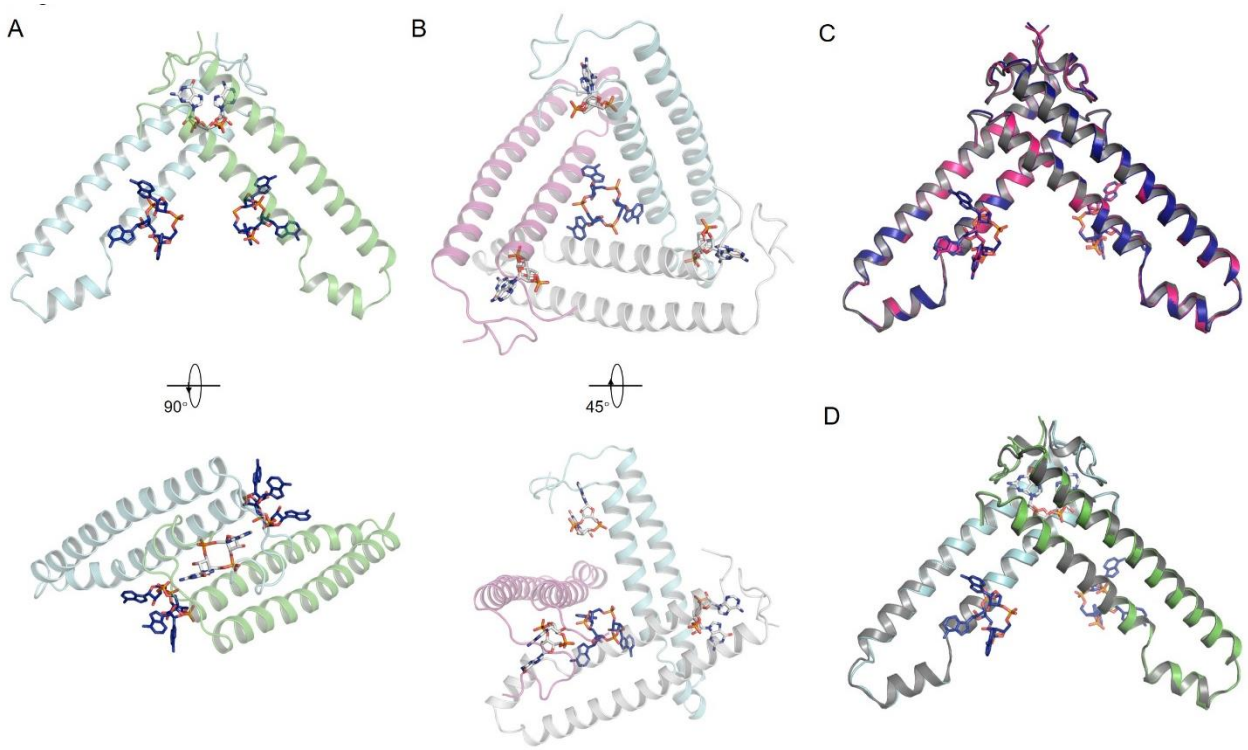

Figure S4. The binding sites of cyclic trinucleotides and dinucleotides are different, related to Figure 2

(A) An Acb2 dimer and the bound 3',3'-cGAMP within the Acb2-3',3'-cGAMP structure is shown. The Acb2-cA_3 structure is aligned to the structure and only the two cA_3 molecules are shown.

(B) An Acb2 trimer and the bound cA_3 within the Acb2-cA_3 structure is shown. The Acb2-3',3'-

cGAMP structure is aligned to the structure and only the three 3',3'-cGAMP molecules are shown.

(C) Structural superimposition among Acb2-cA_3 (colored deep blue), Acb2-cAAG (colored hot pink) and apo Acb2 (colored grey) structures. Only an Acb2 dimer and the cyclic trinucleotides it is binding are shown.

(D) Structural superimposition between Acb2-cA_3-3',3'-cGAMP and apo Acb2 structures. Only an Acb2 dimer and the cyclic nucleotides it is binding are shown.

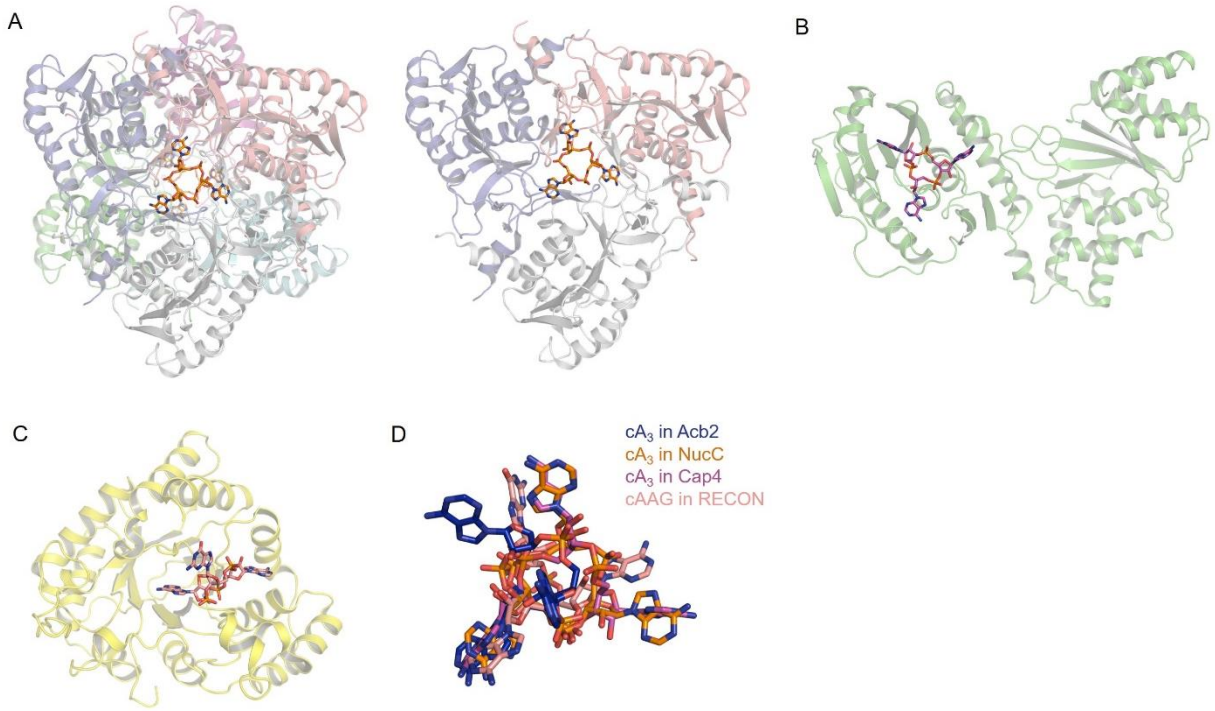

Figure S5. Acb2 binds to cA_3 with a novel fold, related to Figure 3

(A) The binding of cA_3 in NucC from *Escherichia coli* (PDB code: 6P1H). A NucC hexamer bound with two cA_3 molecules and a NucC trimer bound with one cA_3 molecule are shown in the left and right, respectively.

(B) The binding of cA_3 in Cap4 from *Acinetobacter baumannii* (PDB code: 6WAN).

(C) The binding of cAAG in RECON from *Mus musculus* (PDB code: 6M7K).

(D) cA_3 and cAAG molecules in the structures of Acb2-cA_3, NucC-cA_3, Cap-cA_3 and RECON-cAAG are aligned together and highlighted.

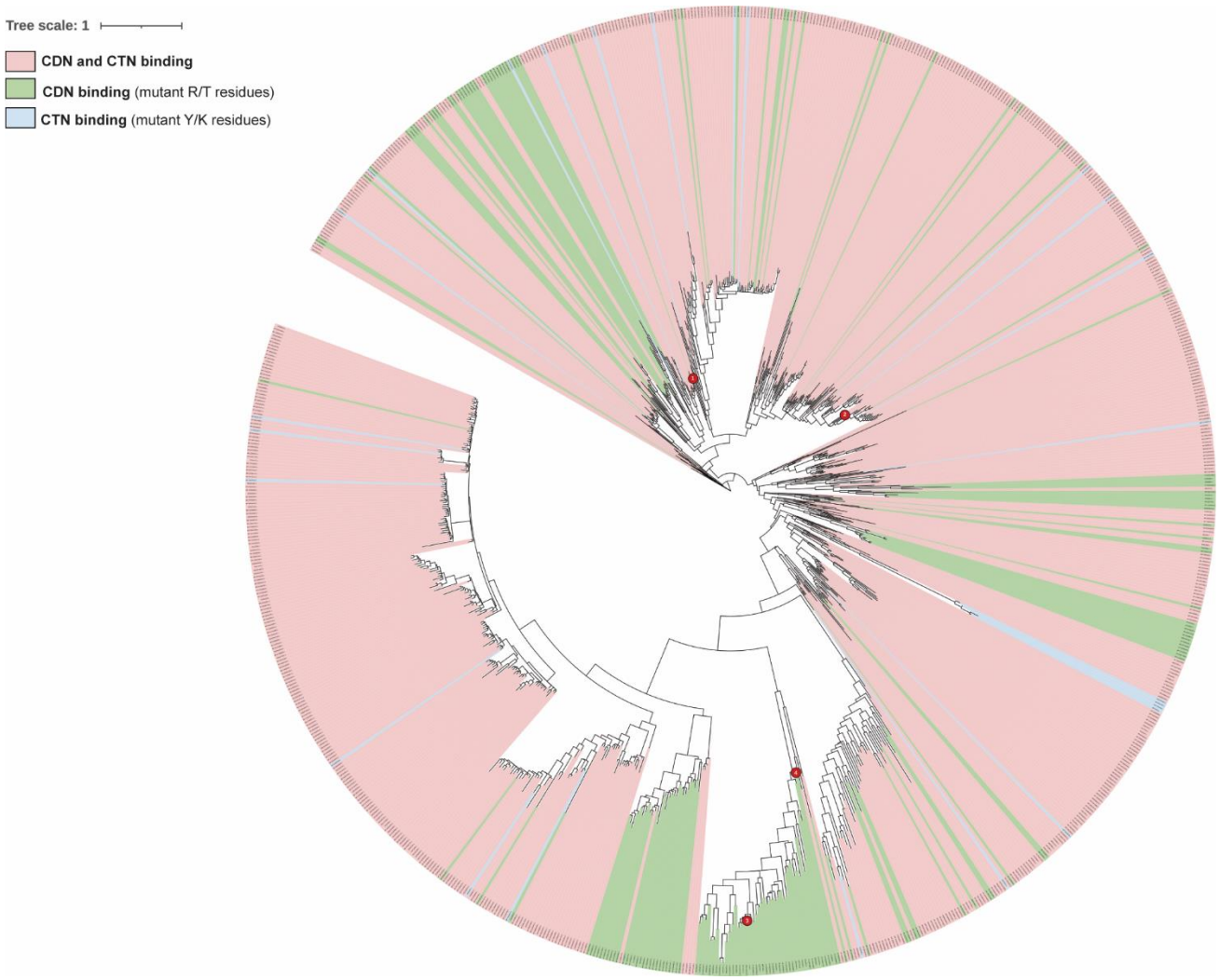

Figure S6. Phylogenic analysis of unique Acb2 homologs across the genomes of prokaryotes and prokaryotic viruses, related to Figures 4 and 5.

Phylogenetic tree of all 878 unique Acb2 protein sequences and classified based on the ability of Acb2 to accommodate CDN and CTN sequences. Branches denoted with the red circles were studied in vitro and/or in vivo: (1) *P. aeruginosa* phage PaMx33, (2) *P. aeruginosa* phage JBD67, (3) *E. coli* phage T4, (4) *Serratia* phage CHI14.

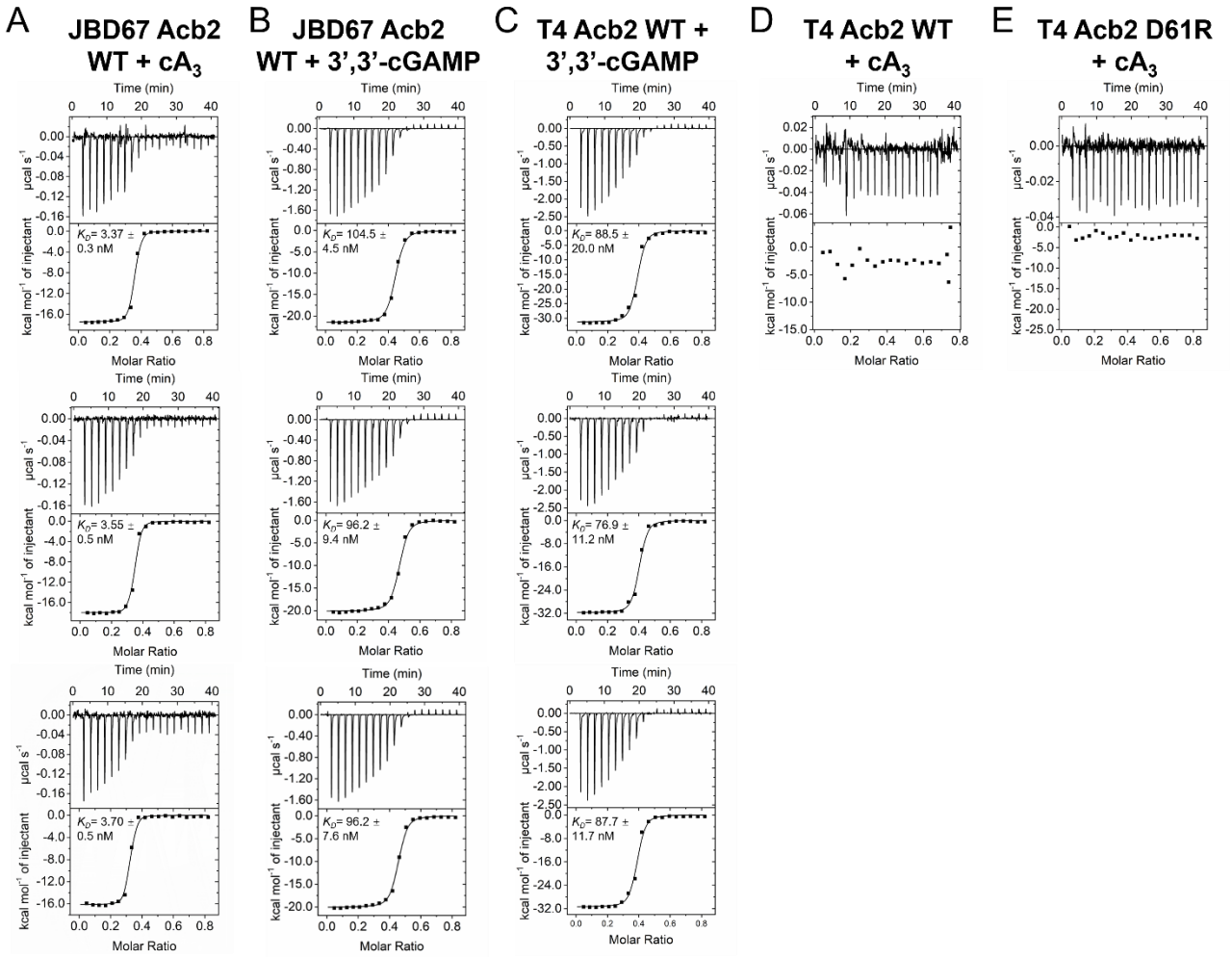

Figure S7. The binding spectrums of JBD67-Acb2 and T4-Acb2 studied by ITC assays, related to Figure 4

(A-B) ITC assays to test binding of cyclic oligonucleotides to JBD67-Acb2.

(C-D) ITC assays to test binding of 3',3'-cGAMP to T4-Acb2.

(E) ITC assays to test binding of cA_3 to T4-Acb2 D61R.

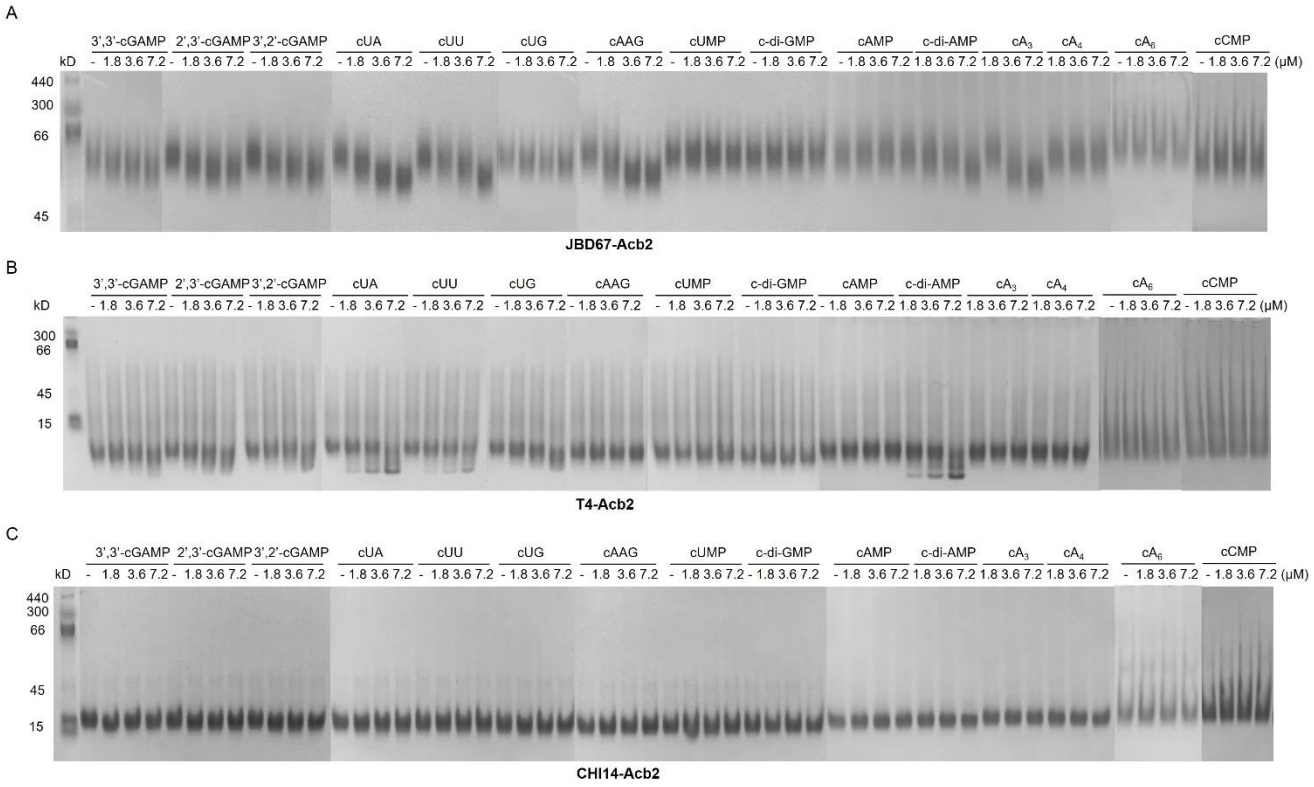

Figure S8. The binding spectrums of Acb2 homologs studied by native PAGE, related to Figure 4

(A-C) Native PAGE assay showed the binding of cyclic nucleotides to JBD67-Acb2, T4-Acb2 and CHI14-Acb2. The proteins were incubated with small molecules at indicated concentrations. Then the samples were subjected to native PAGE.

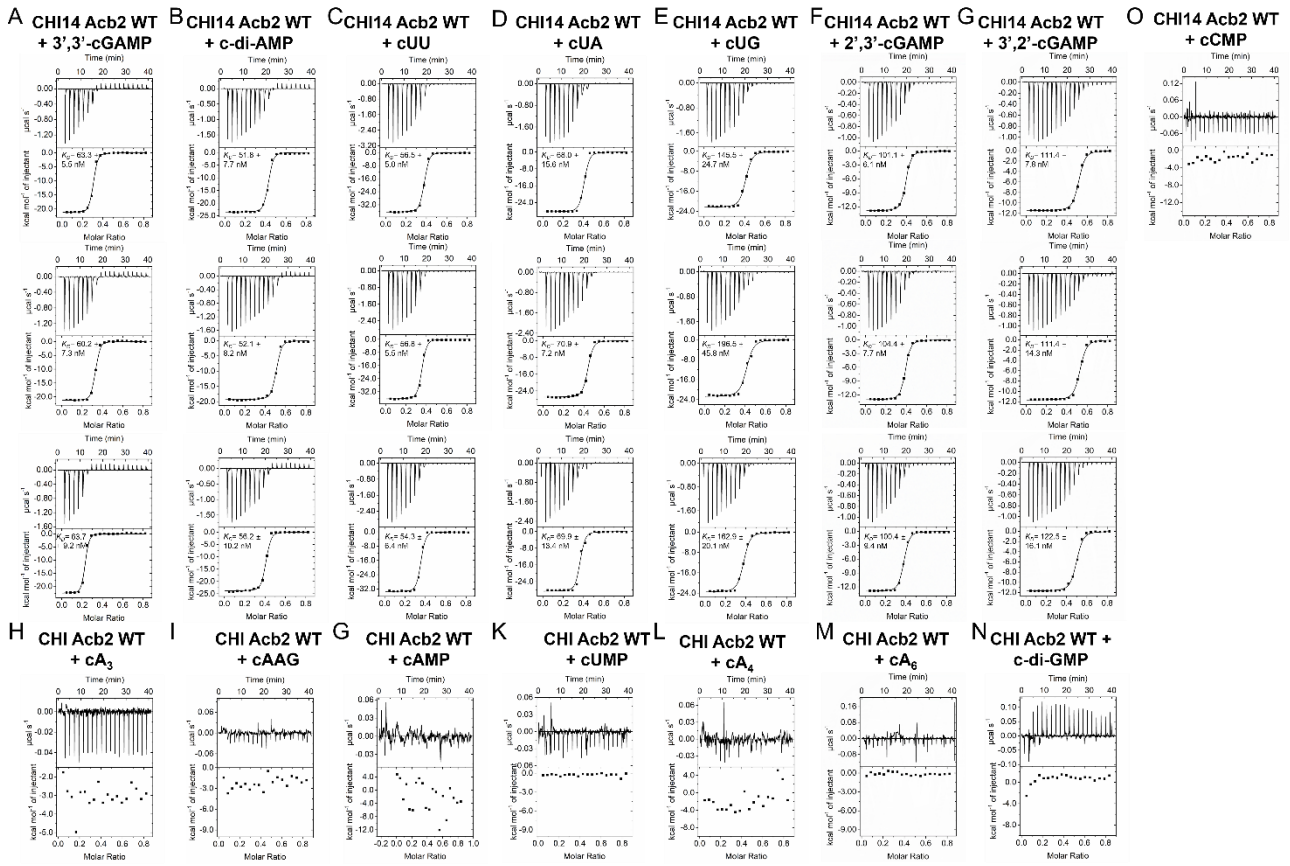

Figure S9. The binding spectrum of CHI14-Acb2 studied by ITC assays, related to Figure 4

(A-O) ITC assays to test binding of cyclic nucleotides to CHI14-Acb2.

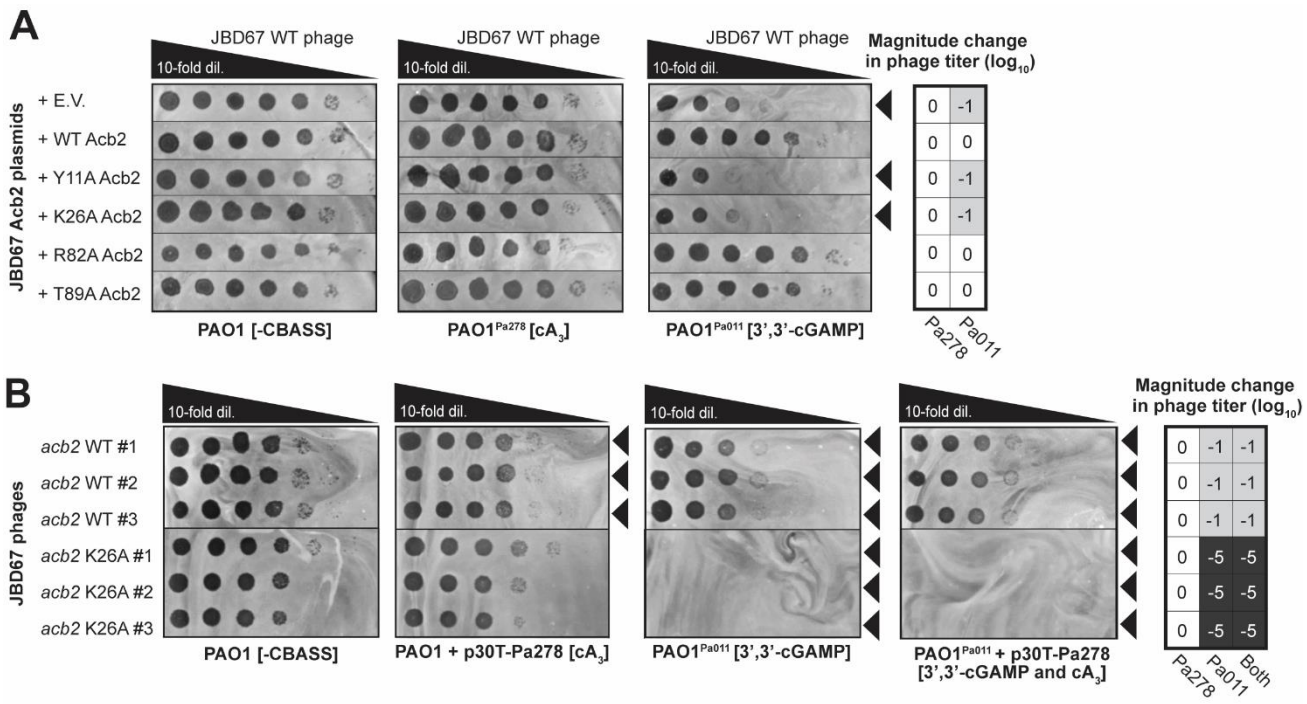

Figure S10. Mutations in Acb2 binding residues differentially impacts phage titer related to Figure 5. (A) Plaque assays with JBD67 WT phage spotted in 10-fold serial dilutions on PAO1 strains harboring an empty vector (E.V.) plasmid or JBD67 Acb2 variants. The PAO1 strains either contain no CBASS operon (-CBASS), a chromosomally integrated Pa011 CBASS operon ($PAO1^{Pa011}$), or a chromosomally integrated Pa278 CBASS operon ($PAO1^{Pa278}$). These plaque assays were used to quantify the order of magnitude change in phage titer by comparing the number of spots (with plaques, or clearings if plaques were not visible) on the $PAO1^{Pa011}$ or $PAO1^{Pa278}$ CBASS-expressing strains divided by the PAO1 (-CBASS) strain (n=3). Basal expression of the Pa011 CBASS operon and 0.3mM IPTG-inducible expression of the Pa278 CBASS operon is sufficient for phage targeting. Black arrowheads highlight significant CBASS-dependent reductions in phage titer. (B) Plaque assays with JBD67 phages spotted in 10-fold serial dilutions on PAO1 strains with and without CBASS: PAO1 + p30T-E.V. (-CBASS), PAO1 + p30T-Pa278, $PAO1^{Pa011}$ + p30T-E.V., $PAO1^{Pa011}$ + p30T-278. These plaque assays were used to quantify the order of magnitude change in phage titer (n=3). Basal expression of the Pa278 CBASS operon is sufficient for phage targeting. Black arrowheads highlight significant CBASS-dependent reductions in phage titer.